

Forward neutrino production and event rates at the Future Circular Collider for hadron collisions

B. R. Ko^a and E. Won^{b,1}

^b*Department of Accelerator Science, Korea University Sejong Campus, 2511 Sejong-ro, Sejong 30019, Republic of Korea*

^b*Department of Physics, Korea University, 145 Anam-ro, Seoul 02841, Republic of Korea*

E-mail: eunilwon@korea.ac.kr

ABSTRACT: A proposed future ultra high energy collider such as the Future Circular Collider produces intense and collimated neutrinos from weak decays of hadrons. We have estimated the production yields of such neutrinos from proton-proton collisions whose center-of-mass energy is 100 TeV and integrated luminosity of 1 ab^{-1} . Using a hypothetical detector positioned either 0.5 km or 2 km downstream of the proton-proton interaction point along the beamline, we have discussed the expected charged current neutrino scattering event rates and their possible extension up to the neutrino energy of about 50 TeV. We have also addressed a feasibility to observe so-far-unmeasured direct W^\pm boson production from the interactions of neutrinos with nucleus.

KEYWORDS: Neutrinos, Proton Proton Collisions, Weak Decays

¹Corresponding author.

Contents

| | | |
|----------|---------------------------------|----------|
| 1 | Introduction | 1 |
| 2 | Neutrino flux estimation | 2 |
| 3 | Neutrino event rates | 6 |
| 4 | Summary | 8 |

1 Introduction

A large part of the particle physics community is dedicating growing efforts towards the construction of higher-energy colliders that exceed the capabilities of the Large Hadron Collider (LHC) [1, 2] to explore physics beyond the Standard Model (SM), which has not yet been evidenced by the ATLAS [3] and CMS [4] experiments. One such proposed facility is the Future Circular Collider (FCC) project [5]. The FCC is subdivided into three collider types: FCC-hh for hadron-hadron collisions (with an option for heavy-ion collisions), FCC-ee for electron-positron collisions, and FCC-eH for electron-hadron collisions. Among these, the FCC-hh is expected to operate at a center-of-mass collision energy of $\mathcal{O}(100)$ TeV with a target average instantaneous luminosity of $\mathcal{O}(10^{35}) \text{ cm}^{-2}\text{s}^{-1}$ [6].

Such high-energy, high-luminosity hadron colliders are known to produce intense neutrino and antineutrino beams via weak hadron decays. At the LHC, neutrino fluxes and corresponding event rates have been estimated [7, 8], and the FASER collaboration has recently reported relevant experimental observations [9, 10]. A recent study [11] broadened these neutrino physics observations by examining various detector configurations at a 100 TeV proton-proton (pp) collider and by outlining their potential to probe new physics.

In this study, we examine configurations involving a FASER ν -like detector, with a mass of approximately 124 kg [10], positioned 0.5 km or 2 km downstream of the pp interaction point along the beamline of the FCC-hh. In addition to evaluating the expected rates of charged current neutrino scattering events for neutrino energy of about 50 TeV, we explore the possibility of observing on-shell W^\pm boson production in neutrino-nucleus interactions, where hadronic coupling is mediated by a virtual photon [12]. This W^\pm boson production mechanism, mediated by a virtual photon, is complementary to W^- production via the Glashow resonance mechanism [13] and, notably, also permits W^+ production. A candidate Glashow resonance event has been reported by the IceCube collaboration [14, 15]. As previously discussed in ref. [11], rigorous tests of the SM involving neutrino interactions—including both deep inelastic scattering and W^\pm production—may provide avenues for probing beyond the SM, such as dark matter candidates, sterile neutrinos, and non-standard neutrino interactions [16].

2 Neutrino flux estimation

Based on 1 ab^{-1} of simulated pp collision data at $\sqrt{s} = 100 \text{ TeV}$, as recorded by a detector at the FCC-hh, we estimated the production yields of forward neutrinos using PYTHIA8 [17, 18] with parton distribution functions (PDFs) obtained from LHAPDF [19]. The `SoftQCD:inelastic` process was employed, as its cross section is largely insensitive to PYTHIA8 parameter tuning and demonstrates good agreement with the measured inelastic pp cross section at $\sqrt{s} = 13 \text{ TeV}$ $\sigma_{\text{inel}} = 78.1 \pm 0.6 \pm 1.3 \pm 2.6 \text{ mb}$ [20]. Since `SoftQCD:inelastic` does not provide explicit cross sections, we estimated the $\sigma_{b\bar{b}X}$ and $\sigma_{\text{prompt } c\bar{c}X}$ ¹ by counting the numbers of charmed and B hadrons in the generated inelastic events. To enable clearer identification of $c\bar{c}X$ events, B hadron decays were disabled during the estimation. The resulting cross section estimates were then compared with those obtained from `HardQCD:hardbbbbar` and `HardQCD:hardccbar`.

We performed the counting procedure using three PYTHIA8 tunes: `Tune:pp=14` [21], 19 [22], and 20. `Tune:pp=14` corresponds to the default configuration in PYTHIA8 whereas `Tune:pp=19` and 20 are derived from the ‘‘ATLAS A14 central tune’’ [22] with `CTEQ6L1` and `MSTW2008LO` from LHAPDF [19], respectively. To improve agreement with measured cross sections [23, 24], the charm quark mass m_c was adjusted from $1.5 \text{ GeV}/c^2$ to $1.0 \text{ GeV}/c^2$. Table 1 presents the predicted cross sections for each tune with modified $m_c = 1.0 \text{ GeV}/c^2$, along with the corresponding experimental data. The explicit cross sections from `HardQCD:hardbbbbar` and `HardQCD:hardccbar` are also included in table 1. To extract the measured cross section $\sigma_{c\bar{c}X}$, we first reproduced the published multiplicative factor of 3.9 [24] using PYTHIA8, with this factor accounting for the extrapolation of $\sigma_{b\bar{b}X}$ to the full phase space. Adopting the same approach, we estimated the corresponding multiplicative factor for $\sigma_{c\bar{c}X}$ in the full phase space to be 4.73, yielding a full-phase-space cross section of 13.43 mb from the measured value of $2840 \pm 3 \pm 170 \pm 150 \mu\text{b}$ [23].

| | measurement | PYTHIA8 | 14 | 19 | 20 |
|------------------------|-------------|--|-------|-------|-------|
| σ_{inel} | 78.1 [20] | <code>SoftQCD:inelastic</code> | 78.05 | 78.05 | 78.05 |
| $\sigma_{c\bar{c}X}$ | 13.43 [23] | <code>SoftQCD:inelastic</code> by the counting | 14.24 | 13.54 | 14.58 |
| | | <code>HardQCD:hardccbar</code> | 5.34 | 9.53 | 12.25 |
| $\sigma_{b\bar{b}X}$ | 0.6 [24] | <code>SoftQCD:inelastic</code> by the counting | 0.83 | 0.79 | 0.99 |
| | | <code>HardQCD:hardbbbbar</code> | 0.35 | 0.60 | 0.53 |

Table 1. Measured and predicted cross sections at $\sqrt{s} = 13 \text{ TeV}$, expressed in mb. The values 14, 19, and 20 refer to the `Tune:pp` options provided by PYTHIA8.

According to the results in table 1, achieving simultaneous agreement between the predicted $\sigma_{c\bar{c}X}$ and $\sigma_{b\bar{b}X}$ values and experimental measurements is non-trivial. To identify an optimal and valid tuning configuration at the FCC-hh collision energy, we extended the predictions in table 1 to pp collision energies up to 300 TeV, as illustrated in figure 1. The $\sigma_{c\bar{c}X}$ values from `HardQCD:hardccbar` exhibit a strong dependence on tuning parameters

¹We omit the term ‘‘prompt’’ when referring to prompt $c\bar{c}$ events in the following discussion.

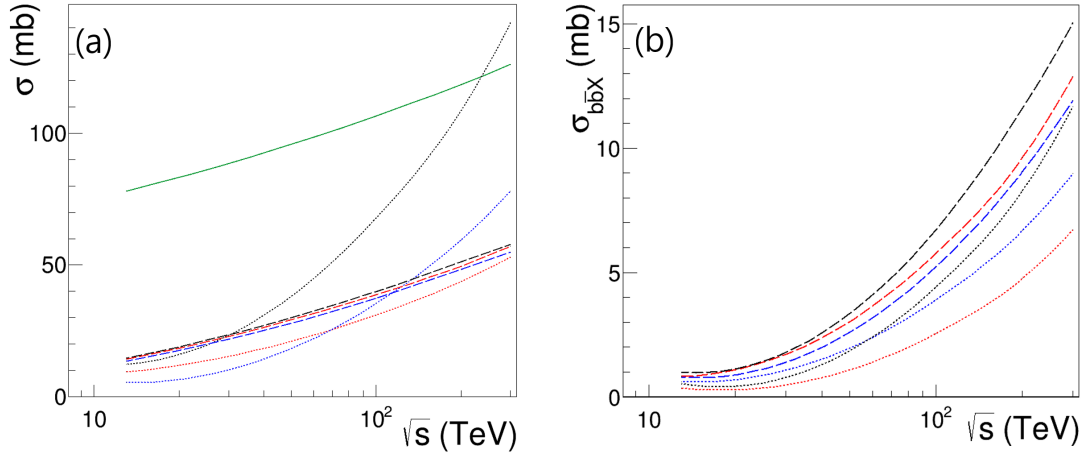


Figure 1. Panels (a) and (b) illustrate $\sigma_{c\bar{c}X}$ and $\sigma_{b\bar{b}X}$ as functions of the pp collision energy \sqrt{s} . The green solid line in panel (a) represents σ_{inel} from `SoftQCD:inelastic`. The dashed lines correspond to cross sections derived from hadron counting, while the dotted lines in panels (a) and (b) represent the values obtained from `HardQCD:hardccbar` and `HardQCD:hardbbbar`, respectively. The red, blue, and black curves denote the results for `Tune:pp=14`, 19, and 20, respectively.

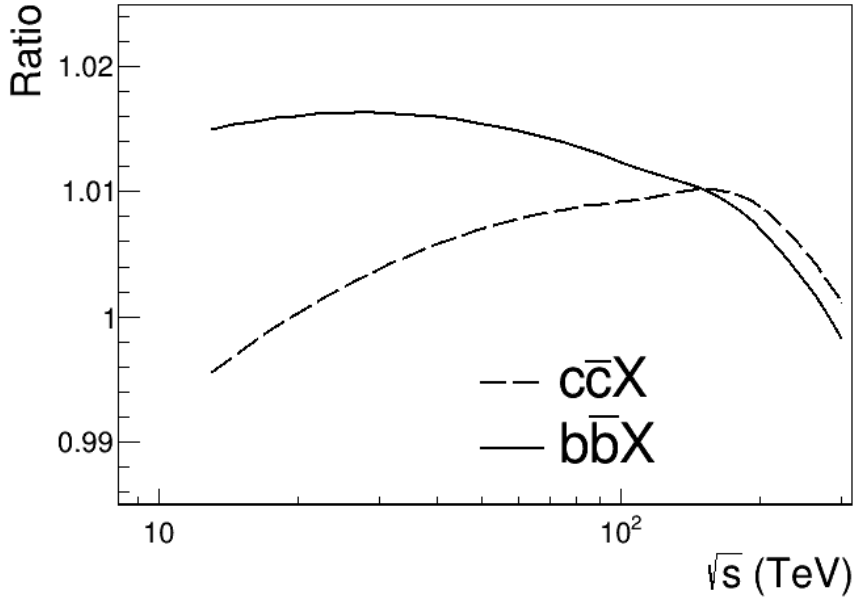


Figure 2. Ratio of cross sections without forward physics tuning to those with it, as a function of \sqrt{s} . The dashed and solid lines represent the ratios for $\sigma_{c\bar{c}X}$ and $\sigma_{b\bar{b}X}$, respectively.

as \sqrt{s} increases, with one configuration yielding an unreasonable $\sigma_{c\bar{c}X}$ that exceeds σ_{inel} . In contrast, the values obtained using our counting method demonstrate reasonable scalability up to \sqrt{s} of 300 TeV, as depicted in figure 1 (a). Meanwhile, the $\sigma_{b\bar{b}X}$ values remain relatively stable across tuning options in PYTHIA8 and do not show notable deviations, as displayed in figure 1 (b). Based on the observed cross section trends in figure 1, we

initially selected `Tune:pp=19` and $m_c = 1 \text{ GeV}/c^2$. We then applied the PYTHIA8 forward physics tuning [25] in combination with this configuration to simulate high-energy neutrino produced along the beamline. As depicted in figure 2, the cross sections obtained with and without the forward physics tuning differ only slightly. Accordingly, all data used for neutrino flux estimation at the FCC-hh energy were generated using `Tune:pp=19`, $m_c = 1 \text{ GeV}/c^2$, and forward physics tuning. The σ_{inel} value of 106.6 mb at $\sqrt{s} = 100 \text{ TeV}$, obtained from `SoftQCD:inelastic`, corresponds to the green solid line in figure 1 (a) and was adopted in this study.

For the neutrino flux estimation, 1×10^9 inelastic pp events were generated at $\sqrt{s} = 100 \text{ TeV}$, and all resulting unstable particles—including muons, pions, kaons, and neutrons—were allowed to decay according to their lifetimes. Neutrinos were required to be produced within 3 cm in the transverse direction, ensuring their production occurred within the beam pipe, in line with [7]. In this study, we constrained the opening angles relative to the beam

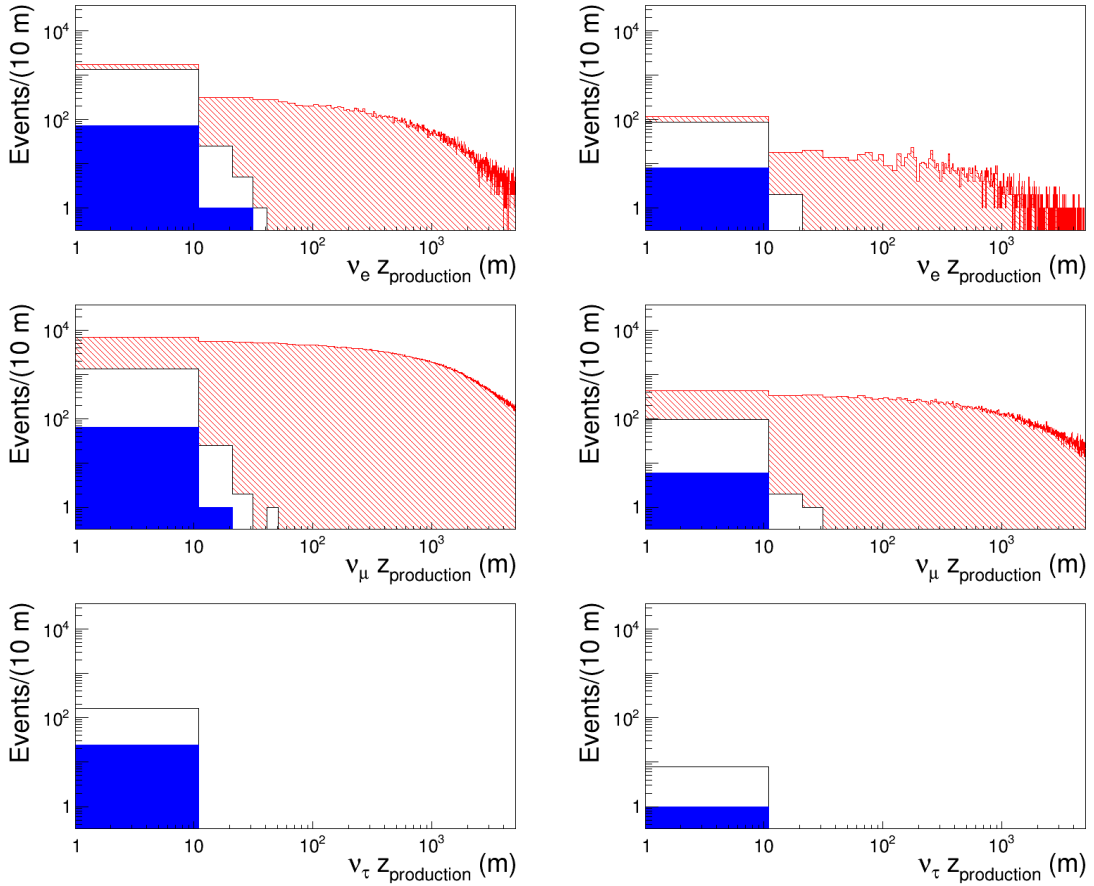


Figure 3. Longitudinal production positions $|z_{\text{production}}|$ for ν_e , ν_μ , and ν_τ , respectively, from top to bottom. Left and right panels show those with the opening angle less than 0.0164 mrad and 0.0041 mrad, respectively. The blue shaded, hollow, and red hatched are contributed from B , charmed, and light particles, respectively.

direction to below 0.0164 mrad and 0.0041 mrad, corresponding to detector locations at 0.5

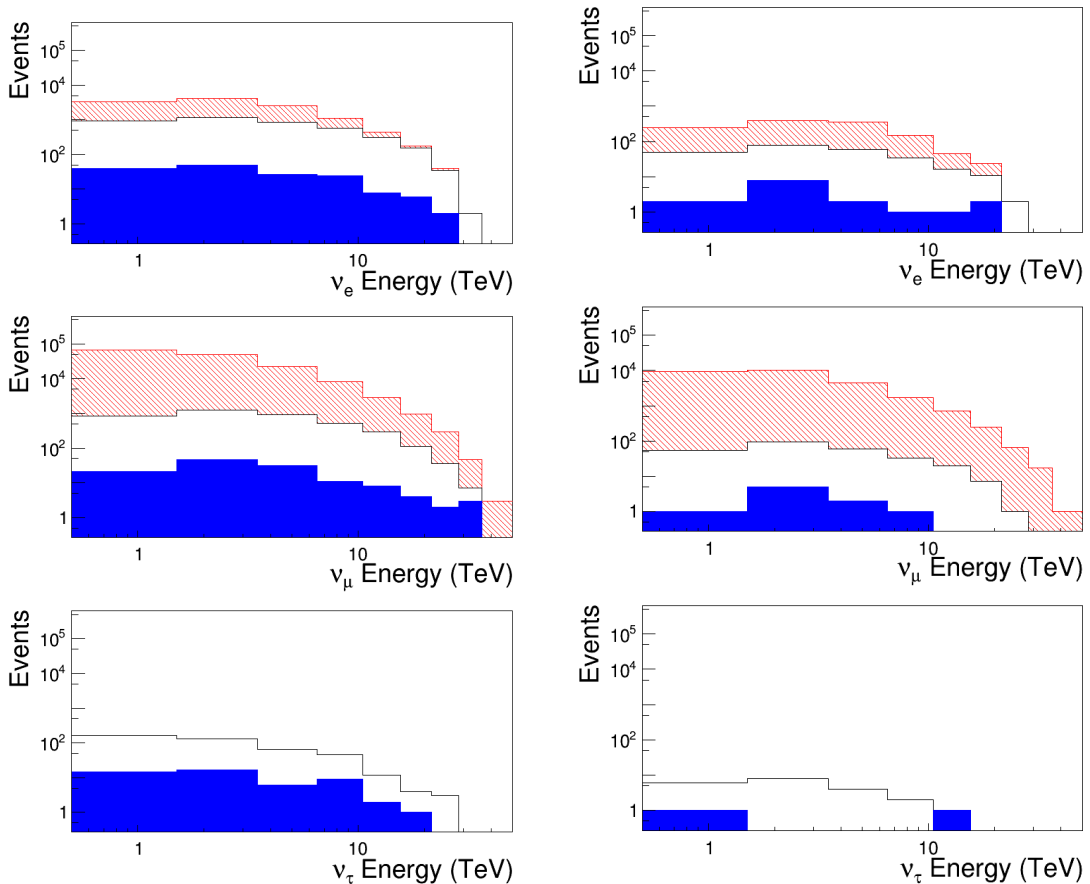


Figure 4. Neutrino energy distributions above 0.5 TeV. Left panel shows those with the opening angle less than 0.0164 mrad and $|z_{\text{production}}| < 0.5$ km and right shows those with 0.0041 mrad and $|z_{\text{production}}| < 2$ km, respectively. The blue shaded, hollow, and red hatched are contributed from B , charmed, and light particles, respectively.

and 2 km from the pp collision point, respectively. A circular detection area with a radius of 8.2 cm was assumed, approximating the 23.4×9 cm² (≈ 211 cm²) surface area of the FASER ν detector target. Figure 3 illustrates the neutrino production position up to 5 km in both the forward and backward longitudinal directions. According to PYTHIA8, neutrinos produced from heavy-flavor particles, such as charmed and B hadrons, emerge within several tens of meters, whereas those from light particles, including pions and kaons, can originate at distances beyond 5 km, as illustrated in figure 3. In this simulation, charmed and kaon particles primarily contribute to the ν_e flux, while the ν_μ flux is dominated by charmed, kaon, and pion particles. Assuming that a FASER ν -like detector is positioned 0.5 or 2.0 km downstream of the pp collision point, figure 4 depicts the incoming neutrino energy spectra, which extend up to approximately 50 TeV. Based on an integrated luminosity of 1 ab^{-1} over one year at the FCC-hh [6], the resulting neutrino fluxes incident on the detector target are listed inclusively in table 2 for neutrinos with energies above 0.5 TeV.

| | $\theta < 0.0164$ mrad and $0 < z_{\text{production}} < 0.5$ km | $\theta < 0.0041$ mrad and $0 < z_{\text{production}} < 2$ km |
|------------|--|--|
| ν_e | 6.18×10^{11} | 0.64×10^{11} |
| ν_μ | 80.27×10^{11} | 14.34×10^{11} |
| ν_τ | 0.23×10^{11} | 0.01×10^{11} |

Table 2. Estimated numbers of neutrinos under different constraints at the FCC-hh, assuming equal production rates in the forward and backward regions and an integrated luminosity of 1 ab^{-1} over one year. The opening angle θ is defined with respect to the beam direction.

3 Neutrino event rates

To estimate the charged current neutrino interactions in the forward region, we considered a FASER ν -like detector equipped with tungsten targets. The detector had a circular cross-sectional area of approximately 211 cm^2 and a length of 31.6 cm , corresponding to a total target mass of 128.44 kg . This configuration resulted in a target nucleon surface density of approximately $N_T \approx 3.65 \times 10^{26} \text{ nucleons/cm}^2$ and may have enabled the use of the detection efficiencies employed by FASER [10]. The charged current neutrino scattering cross section per nucleon σ was evaluated using [26]

$$\sigma = \frac{\mathcal{N}}{\Phi N_T \epsilon}, \quad (3.1)$$

where $\sigma = \sigma_\nu + \sigma_{\bar{\nu}}$ denotes the sum of the neutrino and antineutrino cross sections per nucleon, \mathcal{N} denotes the neutrino event rate, Φ is the incident neutrino flux for the assumed integrated luminosity (e.g., the values in table 2), and ϵ is the overall detection efficiency. The neutrino event rates \mathcal{N} were estimated as a function of neutrino energy E in the range

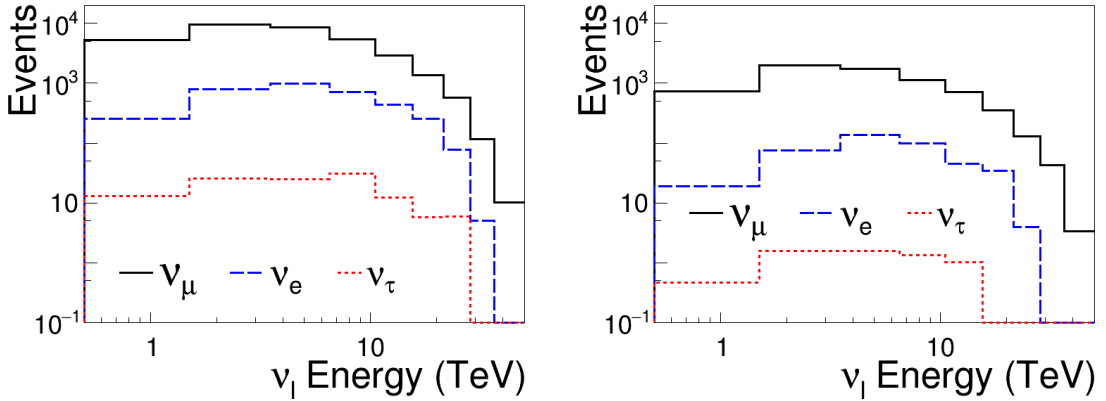


Figure 5. Expected numbers of the charged current interactions for ν_μ (black solid), ν_e (blue dashed), and ν_τ (red dotted), respectively, of scattered neutrino energy. The left and right panels are the cases with the detector locations of 0.5 and 2 km, respectively.

0.5 to 50 TeV, using the established relation $\sigma/E = 1.0 \times 10^{-38} \text{ cm}^2 \cdot \text{GeV}^{-1}$. As previously described, a detection efficiency of $\epsilon = 0.4$ [10] was adopted to reflect the FASER ν -like

detector configuration employed in this study. In the absence of dedicated efficiency values for the ν_τ interactions, the same efficiency was conservatively assumed for ν_τ events. To examine the dependence of event rates \mathcal{N} on the detector placement, two locations—0.5 km and 2 km away from the FCC-hh pp interaction point—were considered. Figure 5 displays the charged current neutrino event rates for ν_μ (black solid lines), ν_e (blue dashed lines), and ν_τ (red dotted lines), as functions of the scattered neutrino energy, from top to bottom. The left and right panels correspond to the detector locations at 0.5 and 2 km, respectively. As illustrated in figure 5 and consistent with the incoming neutrino fluxes shown in figure 4, the charged current ν_μ event rates are expected to reach energies approaching 50 TeV. Although higher energy neutrinos tend to be produced farther from the interaction point, the corresponding event rates are reduced owing to the smaller opening angle resulting from the detector’s limited detection area, as illustrated in figures 4 and 5.

To validate the estimations presented in figure 5, we repeated the procedure using the FASER parameters to reproduce the neutrino event rates reported by the FASER collaboration [10]. The parameters adopted were $\sqrt{s} = 13.6$ TeV, an integrated luminosity of 9.5 fb^{-1} , and an inelastic cross section $\sigma_{\text{inel}} = 78.58 \text{ mb}$ at $\sqrt{s} = 13.6$ TeV, which corresponds to the green solid line in figure 1 (a). As depicted in figure 6, our predicted

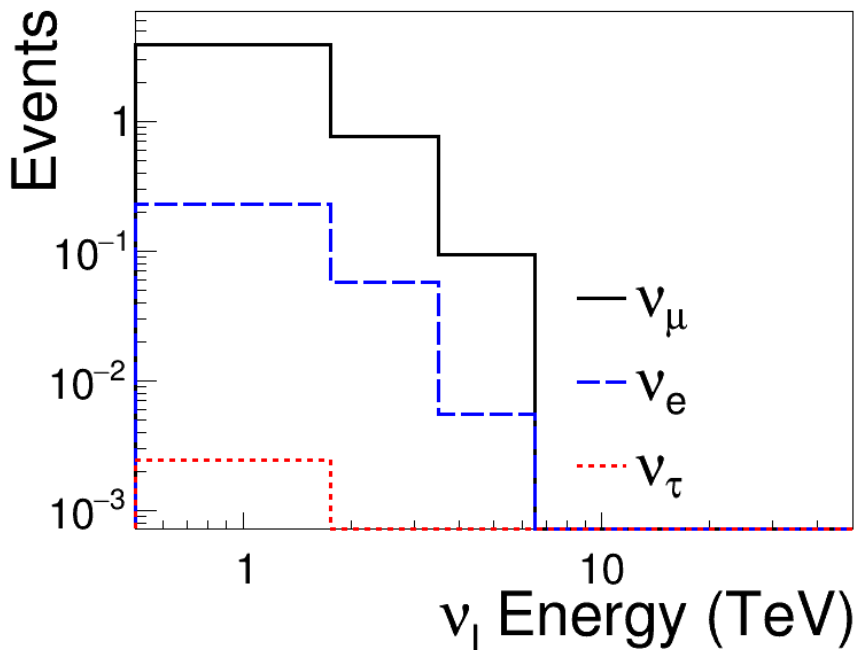


Figure 6. Expected charged interactions for ν_e (dashed), ν_μ (solid), and ν_τ (dotted), respectively, of scattered neutrino energy, with our assumed FASER geometry.

event numbers are approximately 4 for ν_μ and 0.2 for ν_e in the relevant energy range. These are neither substantially overestimated nor underestimated compared with the FASER-reported values of $8 \nu_\mu$ and $4 \nu_e$ events [10]. This level of agreement supports the consistency and credibility of our charged current neutrino event rate estimations shown in figure 5.

Using the same experimental parameters applied to estimate the neutrino event rates in

figure 5, we also evaluated direct W^\pm boson production from neutrino-nucleus interactions, where the hadronic coupling is mediated by a virtual photon [12]. In this simulation, we employed the W boson cross sections reported in [12] and assumed an overall detection efficiency of 0.2 to take account for the reconstruction of additional leptons. As illustrated in figure 7, substantial direct W^\pm production is anticipated from ν_μ interactions at the FCC-hh. These results suggest that the FCC-hh may enable on-shell W^- production, providing complementary mechanism to the Glashow resonance, whose energy threshold lies well beyond the FCC-hh’s capability. A candidate Glashow resonance event, with a reported energy of approximately 6 PeV—notably exceeding the FCC-hh energy—has been observed by the IceCube collaboration [14, 15]. Moreover, W^+ production is also expected at the FCC-hh, in contrast to the Glashow resonance, which exclusively produces W^- bosons.

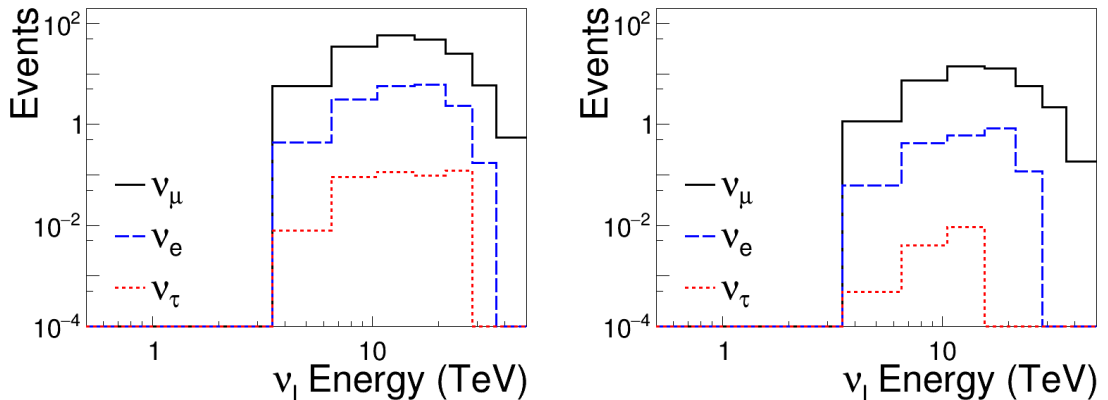


Figure 7. The same as figure 5 except for W^\pm production.

4 Summary

Using a hypothetical detector configuration similar to FASER ν , positioned either 0.5 or 2 km downstream of the pp interaction point along the beamline, and a tuned PYTHIA8 simulation, we estimated forward neutrino production and event rates at the proposed FCC-hh, operating at a pp collision energy of 100 TeV and an integrated luminosity of 1 ab^{-1} . Our findings indicate that charged current neutrino interaction rates can be expected for neutrino energies reaching up to approximately 50 TeV. Moreover, the FCC-hh may offer an opportunity to observe direct W^+ and W^- boson production via neutrino-nucleus interactions, a process that remains to be experimentally quantified. The approach outlined herein can be straightforwardly extended to other detectors with different target masses or alternative placements, through appropriate adjustments to the target volume and opening angle.

Acknowledgments

This work was supported by a Korea University Grant, the National Research Foundation of Korea (NRF) grants funded by the Korea government (MSIT) (RS-2022-NR068913), (RS-2025-00556247), and (RS-2022-00143178), and the Korea Basic Science Institute (National research Facilities and Equipment Center) grant funded by the Korea government (MSIT) (NFEC-2019R1A6C1010027).

References

- [1] LHC Study Group, *Design study of the Large Hadron Collider (LHC)*, CERN 91-03.
- [2] LHC Study Group, *The Large Hadron Collider: conceptual design*, CERN-AC-95-05.
- [3] ATLAS Collaboration, *The ATLAS experiment at the CERN Large Hadron Collider*, JINST 3 (2008) S08003.
- [4] CMS Collaboration, *The CMS experiment at the CERN LHC*, JINST 3 (2008) S08004.
- [5] M. Benedikt *et al.*, *Future Circular Collider Feasibility Study Report Volume 1: Physics, Experiments, Detector*, CERN physics reports, CERN-FCC-PHYS-2025-0002, DOI 10.17181/CERN.9DKX.TDH9, Geneva, 2025. Available online: <https://cds.cern.ch/record/2928193>
- [6] M. Benedikt, X. Buffat, D. Schulte, F. Zimmermann, *LUMINOSITY TARGETS FOR FCC-hh*, Proceedings of IPAC2016, Busan, Korea.
- [7] HyangKyu Park, *The estimation of neutrino fluxes produced by proton-proton collisions at $\sqrt{s} = 14$ TeV of the LHC*, J. High Energ. Phys. **10** (2011) 092.
- [8] Felix Kling and Laurence J. Nevay, *Forward neutrino fluxes at the LHC*, Phys. Rev. D **104** (2021) 113008.
- [9] FASER Collaboration, *First Direct Observation of Collider Neutrinos with FASER at the LHC*, Phys. Rev. Lett. **131** (2023) 031801.
- [10] FASER Collaboration, *First Measurement of ν_e and ν_μ Interaction Cross Sections at the LHC with FASER's Emulsion Detector*, Phys. Rev. Lett. **133** (2024) 021802.
- [11] Roshan Mammen Abraham, Jyotismita Adhikary, Jonathan L. Feng, Max Fieg, Felix Kling, Jinmian Li, Junle Pei, Tanjona R. Rabemananjara, Juan Rojo, Sebastian Trojanowski, *FPF@FCC: Neutrino, QCD, and BSM Physics Opportunities with Far-Forward Experiments at a 100 TeV Proton Collider*, [arXiv:2409.02163](https://arxiv.org/abs/2409.02163).
- [12] Bei Zhou and John F. Beacom, *Neutrino-nucleus cross sections for W-boson and trident production*, Phys. Rev. D **101** (2020) 036011.
- [13] Sheldon L. Glashow, *Resonant Scattering of Antineutrinos*, Phys. Rev. **118** (1960) 316-317.
- [14] IceCube Collaboration, *Observation of High-Energy Astrophysical Neutrinos in Three Years of IceCube Data*, Phys. Rev. Lett. **113** (2014) 101101.
- [15] IceCube Collaboration, *A COMBINED MAXIMUM-LIKELIHOOD ANALYSIS OF THE HIGH-ENERGY ASTROPHYSICAL NEUTRINO FLUX MEASURED WITH ICECUBE*, Astrophys. J. **809** (2015) 98.

- [16] Pedro Machado and Bei Zhou, *Neutrino Physics and Astrophysics at Colliders*, FERMILAB-PUB-25-0421-T [[arXiv:2506.20855](https://arxiv.org/abs/2506.20855)].
- [17] T. Sjöstrand, S. Mrenna and P. Skands, *PYTHIA 6.4 physics and manual*, J. High Energ. Phys. **05** (2006) 026.
- [18] T. Sjöstrand, S. Mrenna and P. Skands, *A brief introduction to PYTHIA 8.1*, Comput. Phys. Comm. **178** (2008) 852.
- [19] Andy Buckley *et al.*, *LHAPDF6: parton density access in the LHC precision era*, Eur. Phys. J. C **75** (2015) 132.
- [20] M. Aaboud *et al.* (ATLAS Collaboration), *Measurement of the Inelastic Proton-Proton Cross Section at $\sqrt{s} = 13$ TeV with the ATLAS Detector at the LHC*, Phys. Rev. Lett. **117** (2016) 182002.
- [21] P. Skands, S. Carrazza, and J. Rojo, *Tuning PYTHIA 8.1: the Monash 2013 tune*, Eur. Phys. J. C **74** (2014) 3024.
- [22] ATLAS Collaboration, *ATLAS Pythia 8 tunes to 7 TeV data*, ATL-PHY-PUB-2014-021.
- [23] LHCb Collaboration, *Measurement of prompt charm production cross-sections in pp collisions at $\sqrt{s} = 13$ TeV*, J. High Energ. Phys. **03** (2016) 159, erratum **09** (2016) 013.
- [24] R. Aaij *et al.* (LHCb Collaboration), *Measurement of the b-Quark Production Cross Section in 7 and 13 TeV pp Collisions*, Phys. Rev. Lett. **118** (2017) 052002.
- [25] Max Fieg, Felix Kling, Holger Schulz, and Torbjörn Sjöstrand, *Tuning PYTHIA for forward physics experiments*, Phys. Rev. D **109** (2024) 016010.
- [26] A. Das and T. Ferbel: *Introduction to Nuclear and Particle Physics* (2nd Edition), World Scientific, Singapore, pg. 19.